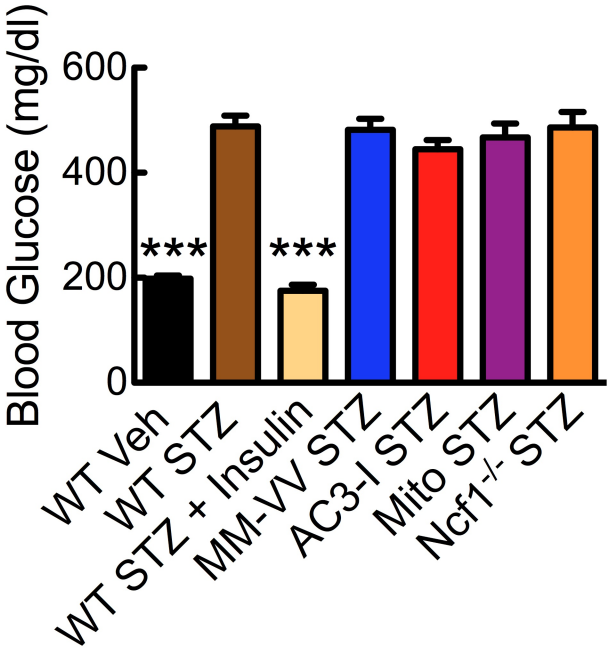

Supplemental Figure 1

STZ causes hyperglycemia. Blood glucose levels after STZ treatment in WT, MM-VV, AC3-I, *Ncf1*$^{-/-}$ and Mito-treated WT mice as well as after Insulin replacement (overall $P < 0.0001$, ***$P < 0.001$, n = 14-38/group). Veh, vehicle; WT, wild type; Mito, MitoTEMPO

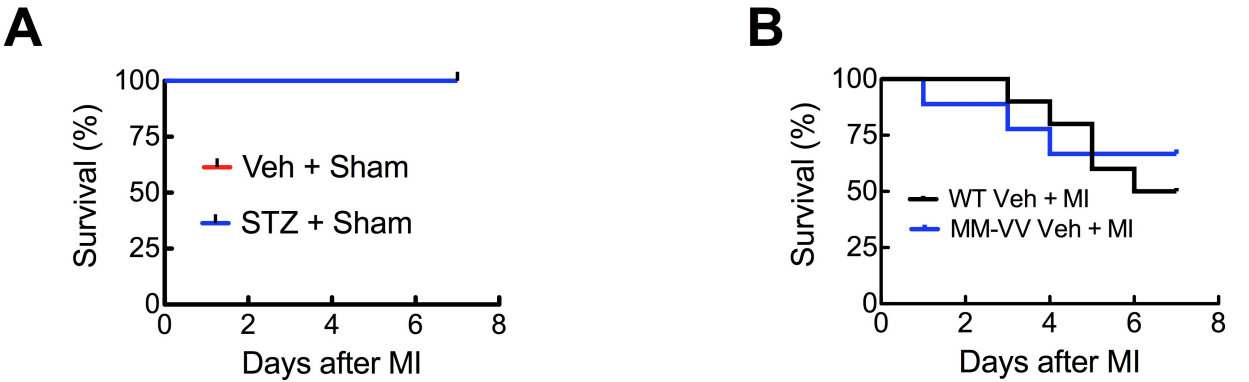

Supplemental Figure 2

Similar survival after sham surgery in diabetic or non-diabetic mice. (A) Survival in WT STZ- and Veh-treated mice after sham surgery, $P = 1.0$ (the red and blue lines are superimposed), $n = 5$/group. **(B)** Similar survival after MI in non-diabetic WT and MM-VV mice, $P = 0.7$, $n = 9$-10/group. WT, wild type; Veh, vehicle.

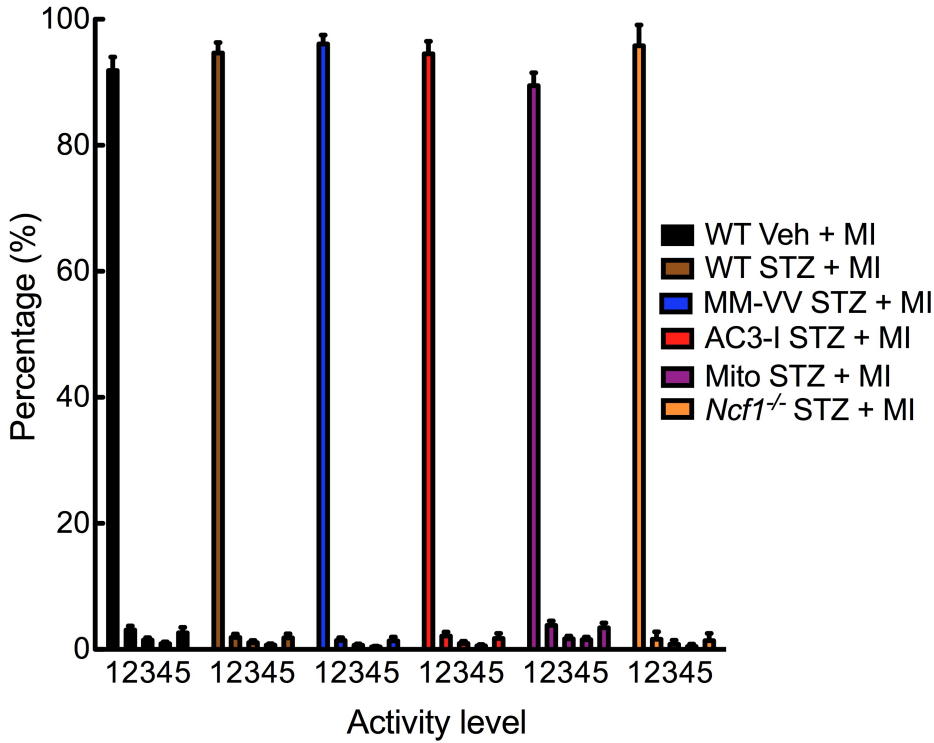

Supplemental Figure 3

Similar activity levels in diabetic and non-diabetic mice after MI. Spontaneous activity levels (1-5) between WT, MM-VV, AC3-I, *Ncf1*$^{-/-}$ or WT + Mito mice after STZ + MI. P = 0.2 for activity 0 (1), P = 0.11 for activity 1-10 (2), P = 0.4 for activity 11-15 (3), P = 0.07 for activity 16-20 (4), P = 0.4 for activity >20 (5), n = 4-10 /group. Veh, vehicle; WT, wild type; Mito, MitoTEMPO

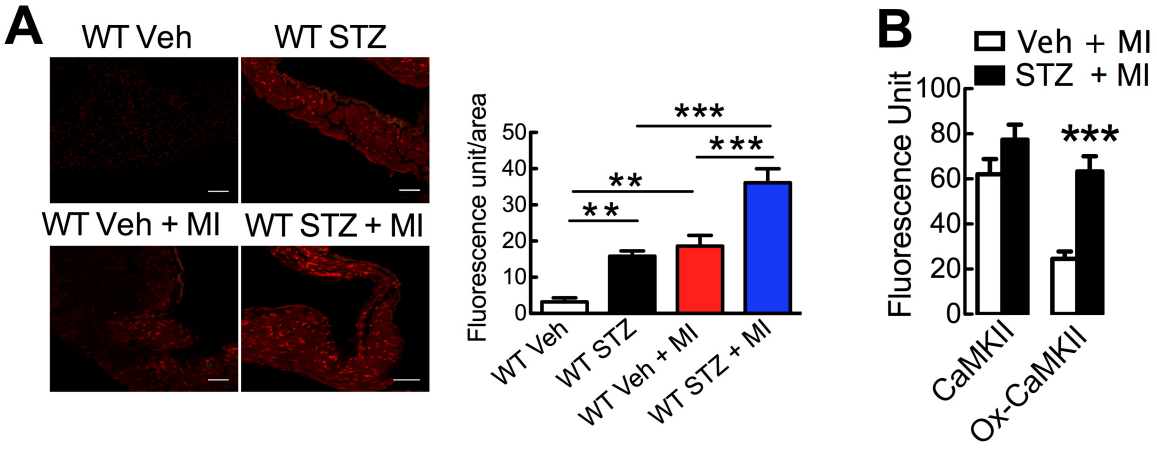

Supplemental Figure 4

Increased ROS and ox-CaMKII in SAN in STZ-treated mice after MI. (**A**) Representative immunofluorescence images of DHE staining in SAN tissues from WT Veh and WT STZ mice with or without MI. Scale bars: 50 μm. Overall $P < 0.0001$ by one way ANOVA, ***$P < 0.001$, **$P < 0.01$ by Neuman-Keumal's test as post hoc study, n = 4-6/group. (**B**) CaMKII ($P = 0.14$) and ox-CaMKII (***$P = 0.0004$) immunostaining in SAN tissues from WT Veh and WT STZ with MI (n = 6/group). Veh, vehicle; WT, wild type;

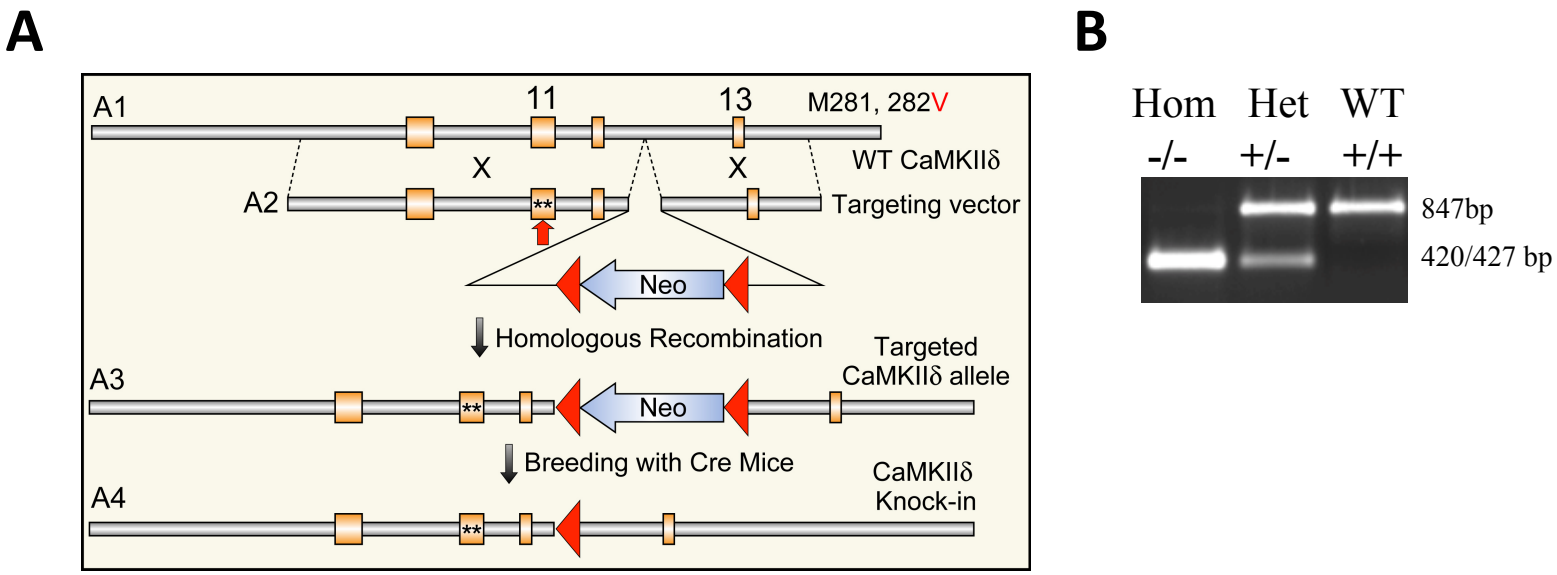

Supplemental Figure 5

Schematic diagram for gene targeting approach for developing MM-VV mice. (**A**) A partial map of the CaMKIIδ gene (A1), the targeting construct (A2), the resulting targeted allele (A3), and the targeted allele after Cre recombination (A4) are shown. In the targeting construct, a 6kb fragment containing exons 9-12 (mutations in Exon 11) and a 4.5-kb fragment containing exon 13 were used as long and short homologous arms, respectively, flanking a LoxP Neo selection marker. (**B**) The knock-in mouse (F3) genotype. The gel showed the HincII–digested PCR products of homozygote (Hom, -/-), heterozygote (Het, +/-) and wild-type (WT, +/+) mice.

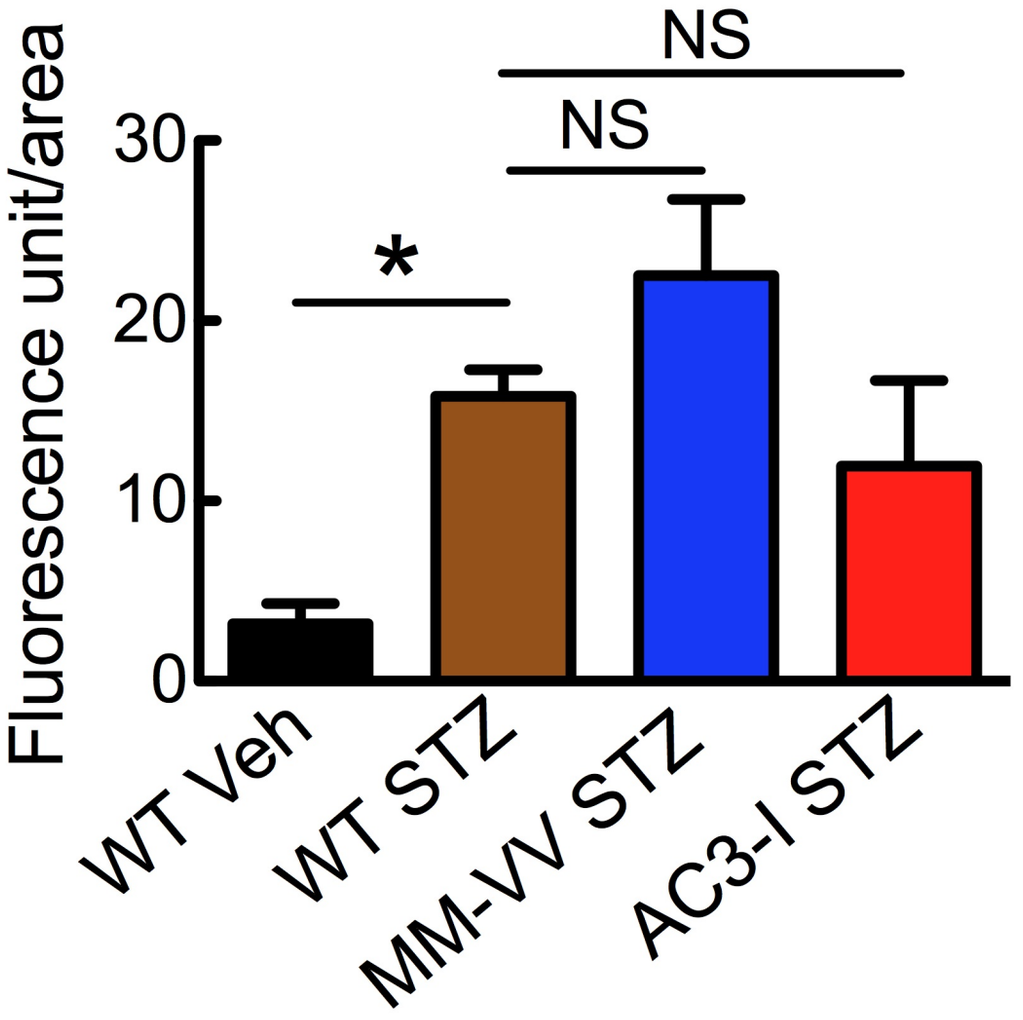

Supplemental Figure 6

ROS in SAN from MM-VV, AC3-I and WT diabetic mice. DHE staining in SAN tissues from Veh- and STZ-treated WT mice, STZ-treated MM-VV and AC3-I mice. Overall $P = 0.0045$, $^*P < 0.05$, $n = 4\text{-}6$/group. NS, not significant. Veh, vehicle; WT, wild type,

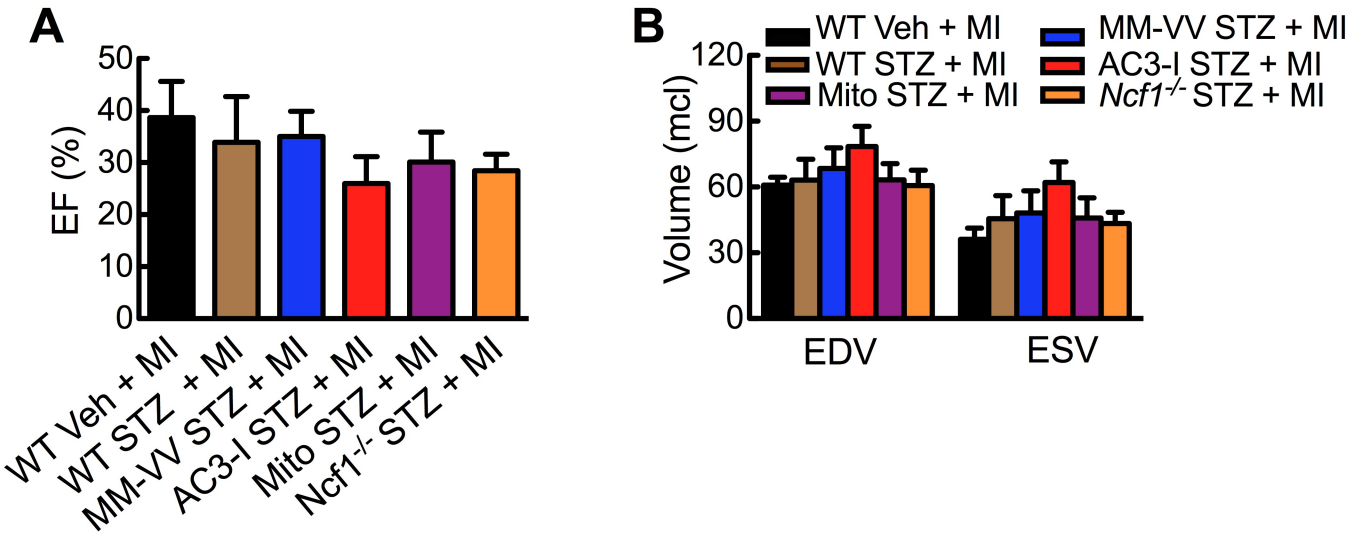

Supplemental Figure 7

Comparable left ventricular contractile function and chamber volumes in non-diabetic (2.1 ± 0.3 days after MI) **and diabetic mice** (2.0 ± 0.4 days after MI)**.** (**A**) Ejection fraction (EF), (**B**) end diastolic volumes (EDV) and end systolic volumes (ESV) after MI in Veh- and STZ-treated WT mice, STZ-treated MM-VV, AC3-I, *Ncf1*$^{-/-}$ or WT + Mito mice. Overall P = 0.6 for EF, overall P = 0.6 for EDV and 0.4 for ESV, n = 4-11/group. Veh, vehicle; WT, wild type; Mito, MitoTEMPO

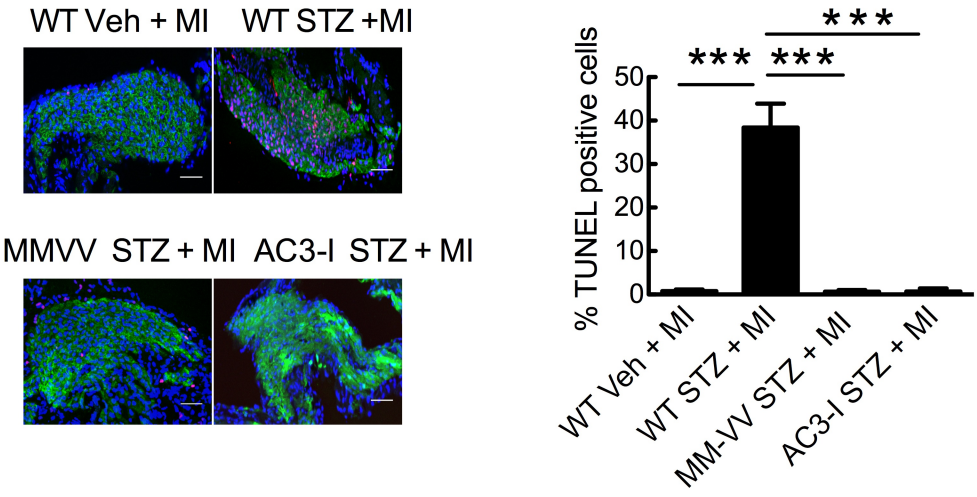

Supplementary Figure 8

Increased SAN apoptosis after MI in STZ-treated WT mice, but not MM-VV or AC3-I mice. Representative immunofluorescence images of TUNEL staining in SAN from WT mice treated with Veh + MI or STZ + MI, MM-VV and AC3-I with STZ + MI (Blue, DAPI; Green, HCN4; Red, TUNEL). Scale bars: 50 μm. Overall $P < 0.0001$, ***$P < 0.001$, n = 4-8/group. Veh, Vehicle; WT, wild type

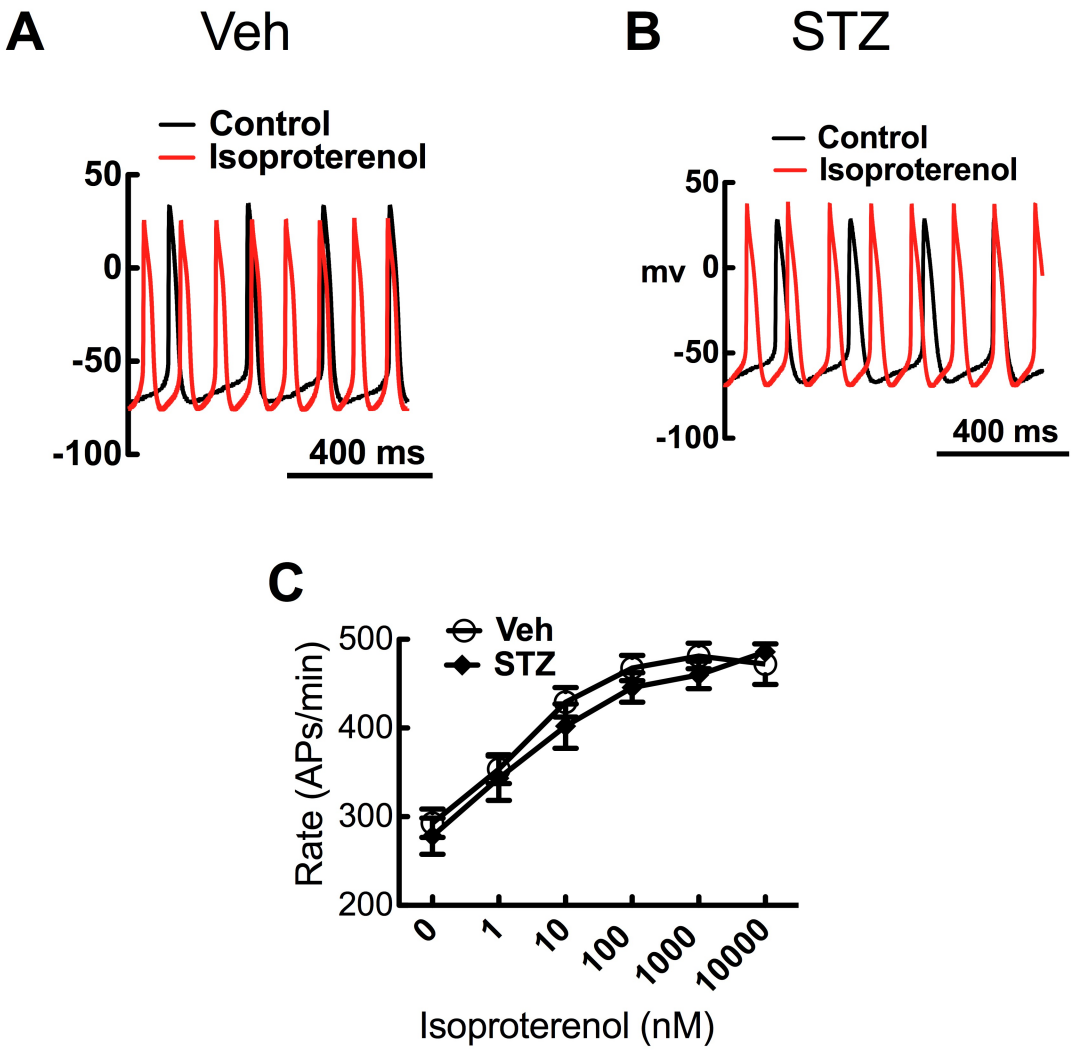

Supplemental Figure 9

STZ does not affect spontaneous or isoproterenol-stimulated automaticity in isolated SAN cells. (**A, B**) Representative tracings of spontaneous action potentials from SAN cells isolated from Veh- and STZ-treated mice with or without isoproterenol. (**C**) Summary data of action potential (AP) rates of SAN cells. $P > 0.05$ between Veh- and STZ-treated group at baseline and after isoproterenol at all doses, n = 7-10 cells/group. Veh, vehicle

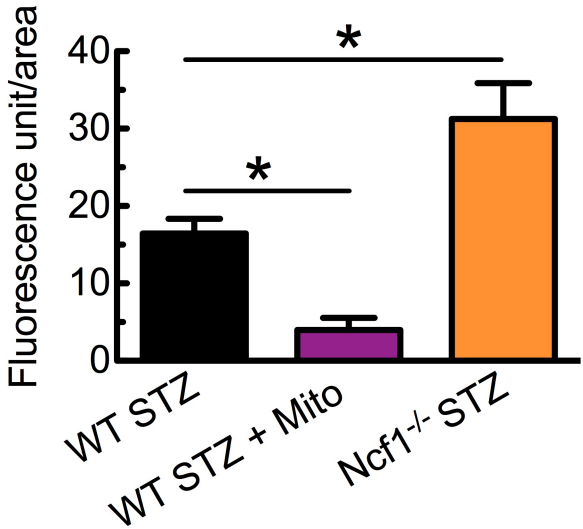

Supplemental Figure 10

Decreased ROS in SAN from MitoTEMPOL-treated mice. DHE staining in SAN from WT mice treated with Mito + STZ, STZ alone and *Ncf1*$^{-/-}$ mice treated with STZ. Overall $P = 0.0003$, $^{*}P < 0.05$, $n = 3\text{-}5$/group. WT, wild type; Mito, MitoTEMPO

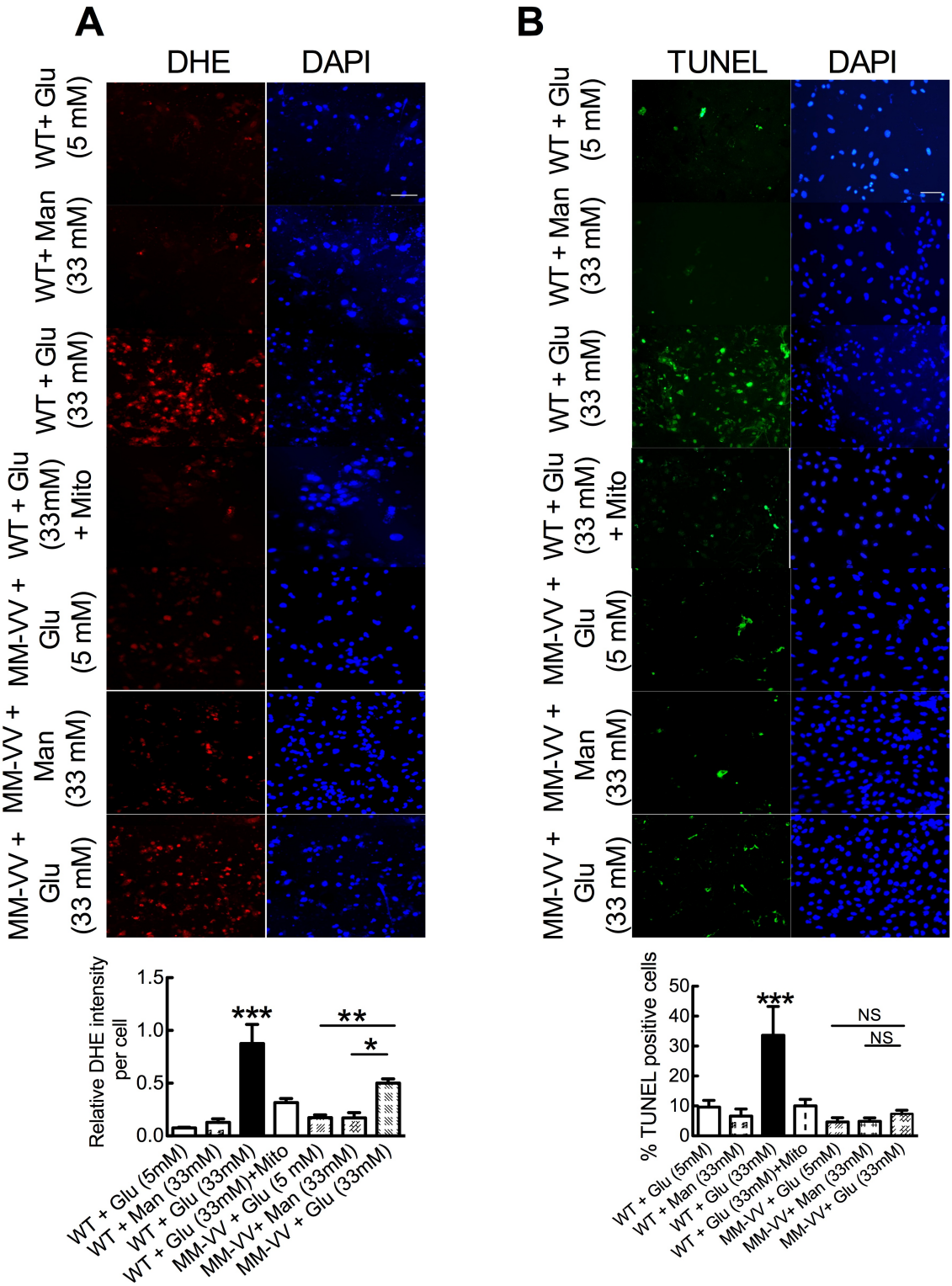

Supplemental Figure 11

Hyperglycemia triggers mitochondrial ROS generation and apoptosis in WT mice but not apoptosis in MM-VV mice. (**A**) DHE staining for ROS in cultured WT neonatal cardiomyocyte treated with glucose (Glu), Glu+Mito (MitoTEMPO, 1 mM) or mannitol (Man) and in MM-VV mice treated with glucose (Glu) or mannitol (Man). (**B**) TUNEL staining in the same experimental groups as in (**A**). For both panels, overall $P < 0.0001$, ***$P < 0.001$ between WT + Glu (33mM) group and all other groups, **$P < 0.01$ and *$P < 0.05$ by Neuman-Keuls test as post hoc study. NS, not significant, n = 3-5 assays/group. WT, wild type

	Vehicle	**STZ**
Body weight (g)	25 ± 0.5	21 ± 0.8*
Heart weight/tibia length (mg/mm)	8.5 ± 0.6	9.2 ± 0.5
Lung weight/tibia length (mg/mm)	8.1 ± 0.4	8.8 ± 0.6
BUN (mg/dl)	24 ± 4	26 ± 1
CO_2 (mEq/l)	15 ± 3.5	14 ± 1.5

Supplemental Table 1. Body weights, organ weights and blood chemistry of vehicle and STZ-treated mice after MI. Body weights (*P < 0.001, n = 24-25/group), lung weights normalized to tibia length (P = 0.4, n = 6-7/group), and heart weights normalized to tibia length (P = 0.4, n = 6-7/group) compared between vehicle- and STZ-treated mice. Serum BUN (P = 0.5, n = 6-8/group) and bicarbonate levels (P = 0.6, n = 5-9 /group) compared between vehicle- and STZ-treated mice.

Echocardiography Parameters	**Veh + MI**	**STZ + MI**	**P**
Ejection Fraction (%)	38.8 ± 0.07	34.0 ± 0.09	0.67
End Diastolic Volumes (ml)	60.8 ± 3.6	63.1 ± 9.5	0.82
End Systolic Volumes (ml)	36.1± 5.1	45.5 ± 10.5	0.41
Stroke volume (ml)	24.7± 3.2	18.0 ± 2.2	0.11
Heart Rate (BPM)	570 ± 33.7	398 ± 51	0.01*
Cardiac output (ml/min)	14.3 ± 2.1	7.1 ± 1.5	0.019 *
Left ventricular mass (mg)	86.4 ± 6.6	80.2 ± 7.0	0.53

Supplemental Table 2. STZ-treated mice had decreased heart rate and cardiac output, but similar contractile function, left ventricular volumes and mass compared to vehicle-treated mice after MI. P values for comparisons between Veh- and STZ-treated mice after MI, n = 7-9/group. Veh, vehicle.

Patient Characteristics	**MI + DM** (n=5)	**MI** (n=5)	**P**
Age (year)	64 ± 7	71 ± 2	0.03
Males (%)	75	60	
Ejection fraction (%)	41 ± 6	35 ± 6	0.5
Type II DM (%)	100	n/a	
Insulin (%)	75	n/a	
Glucose (mg/dl)	260 ± 56	121 ± 13	0.04
Hemoglobin A1C (%)	8.0 ± 0.5	n/a	
Pacemaker (%)	25	0	
ACE inhibitor (%)	80	100	
β−Blocker (%)	100	100	

Supplemental Table 3: Patient characteristics for right atrial tissues shown in Figure 3. ACE, Angiotensin Converting Enzyme.

Cell Type	Source	$R_{gap,\ longitudinal}$	$R_{gap,transverse}$
Atrial	Courtemanche et al. 1998*	1.5 Ωcm^2	15.0 Ωcm^2
Peripheral SAN	Kurata et al. 2008#	*Equation 2*	$R_{gap,long}$
Central SAN	Kurata et al. 2002§	*Equation 2*	$R_{gap,long}$
Block zone	Butters et al. 2010‡	4000 Ωcm^2	$R_{gap,long}$
Inexcitable cell	Morita et al. 2009†	4000 Ωcm^2	$R_{gap,long}$

Supplemental Table 4. Mathematical models for different regions of intact SAN

*Courtemanche et al. *Am J Physiol*. 1998;275:H301-321.

#Kurata et al. *Biophys J*. 2008;95:951-977 with sodium channel conductance = 1.8523×10^{-6} nS/pF.

§Kurata et al. *Am J Physiol Heart Circ Physiol*. 2002;283:H2074-2101.

‡Butters et al. *Circ Res*. 2010;107:126-37. Block zone modeled as coupled region of inexcitable cells with passive leak conductance (E_{leak} = -70 mV).

†Morita et al. *Am J Physiol Heart Circ Physiol*. 2009;297:H1594.

State variable	Definition	Initial value
m	Na^+ current activation gate	0.004147463955
h	Na^+ current inactivation gate	0.9421032891
j	Na^+ current slow inactivation gate	0.9319148046
d	L-type Ca^{2+} current activation gate	0.0001793553646
f	L-type Ca^{2+} voltage-dependent inactivation gate	0.8466729054
f_{ca}	L-type Ca^{2+} calcium-dependent inactivation gate	0.5727907784
X_r	Rapidly activating K^+ current activation gate	0.02303434883
X_s	Slowly activating K^+ current activation gate	0.03616188931
oa	Transient outward K^+ current activation gate	0.03436021906
oi	Transient outward K^+ current inactivation gate	0.9987671846
ua	Ultrarapid rectifier K^+ current activation gate	0.006237057018
ui	Ultrarapid rectifier K^+ current inactivation gate	0.9891443725
u	Ryanodine receptor Ca^{2+} release activation gate	4.537711703e-16
v	RyR Ca^{2+} release inactivation gate	1.0
w	RyR Ca^{2+} release inactivation gate	0.9990895327
$[Ca^{2+}]_i$	Ca^{2+} concentration in myoplasm (mM)	0.0002599348619
$[Ca^{2+}]_{JSR}$	Ca^{2+} concentration in junctional SR (mM)	0.4298392427
$[Ca^{2+}]_{NSR}$	Ca^{2+} concentration in network SR (mM)	1.960512954
$[Na^+]_i$	Na^+ concentration in myoplasm (mM)	15.19468146
$[K^+]_i$	K^+ concentration in myoplasm (mM)	134.9547735
V_m	Transmembrane potential (mV)	-79.01495665

Supplemental Table 5. Initial conditions for state variables in mathematical model of atrial action potential*.**Single cell was paced to steady-state at cycle length = 300 ms. Model equations for human atrial cell model are found in original publication (1). SR, sarcoplasmic reticulum.*

State variable	Definition	Initial value (Central)	Initial value (Peripheral)
m	Na^+ current activation gate	-	0.0690372072
h	Na^+ current inactivation gate	-	0.2223618089
j	Na^+ current slow inactivation gate	-	0.01430146964
d	L-type Ca^{2+} current activation gate	0.0006779558663	4.66775128e-05
f	L-type Ca^{2+} voltage-dependent inactivation gate	0.6621880012	0.459162836
f_{ca}	L-type Ca^{2+} calcium-dependent inactivation gate	0.5710787057	0.4667391842
$X_{r,f}$	Rapidly activating K^+ current fast activation gate	0.3160790736	0.5254608664
$X_{r,s}$	Rapidly activating K^+ current slow activation gate	0.6156126509	0.6219289422
$X_{r,i}$	Rapidly activating K^+ current inactivation gate	0.847082724	0.933848794
n	Slowly activating K^+ current activation gate	0.0552203568	0.07350047887
q	Transient outward K^+ current activation gate	0.5239671546	0.5779873691
r	Transient outward K^+ current inactivation gate	0.005795549972	0.00199964719
dt	T-type Ca^{2+} current activation gate	0.005151304518	0.0003472296223
ft	T-type Ca^{2+} current inactivation gate	0.2498661863	0.3016670853
qa	Sustained inward current activation gate	0.4591365202	-
qi	Sustained inward current inactivation gate	0.3860293202	-
y	Pacemaker (funny) current activation gate	0.02836884815	0.01632643918

$[Ca^{2+}]_i$	Ca^{2+} concentration in myoplasm (mM)	0.00023567935	0.0002461860556
$[Ca^{2+}]_{JSR}$	Ca^{2+} concentration in junctional SR (mM)	0.3477078758	0.219459533
$[Ca^{2+}]_{NSR}$	Ca^{2+} concentration in network SR (mM)	2.518529555	4.245147564
$[Na^{+}]_i$	Na^{+} concentration in myoplasm (mM)	9.211637929	7.679366896
$[K^{+}]_i$	K^{+} concentration in myoplasm (mM)	140.1632028	141.5993186
V_m	Transmembrane potential (mV)	-57.88001647	-74.11420057

Supplemental Table 6. Initial conditions for state variables in mathematical models of central and peripheral SAN cells*. **Single cell underwent spontaneous activity for 10 seconds. Model equations for rabbit central and peripheral node cells are found in original publication (2). SR, sarcoplasmic reticulum*

Supplemental equations for mathematical modeling as below:

Capacitive membrane area (cm^2)

x is distance in cm.

$$A_{cap} = 110 \times 10^{-6} - 45 \times 10^{-6}\left(\frac{1}{1+exp(-4(x-7.0))} + \frac{1}{1+exp(4(x-9.0))}\right) \quad [1]$$

Gap junction resistance (Ωcm^2)

$$R_g = 110\left(\frac{1}{1+exp(-4(x-7.0))} + \frac{1}{1+exp(4(x-9.0))}\right) - 108.5 \quad [2]$$

Conductance of fast sodium current (mS/cm^2)

$$\bar{g}_{Na} = 3.7 \times 10^{-6} - 1.85 \times 10^{-6}\left(\frac{1}{1+exp(-5(x-6.5))} + \frac{1}{1+exp(5(x-9.5))}\right) \quad [3]$$

References:

1. Courtemanche, M., Ramirez, R.J., and Nattel, S. 1998. Ionic mechanisms underlying human atrial action potential properties: insights from a mathematical model. American Journal of Physiology 275:H301-321.
2. Kurata, Y., Matsuda, H., Hisatome, I., and Shibamoto, T. 2008. Regional difference in dynamical property of sinoatrial node pacemaking: role of na+ channel current. Biophys J 95:951-977.

Full unedited gel for Figure 3A

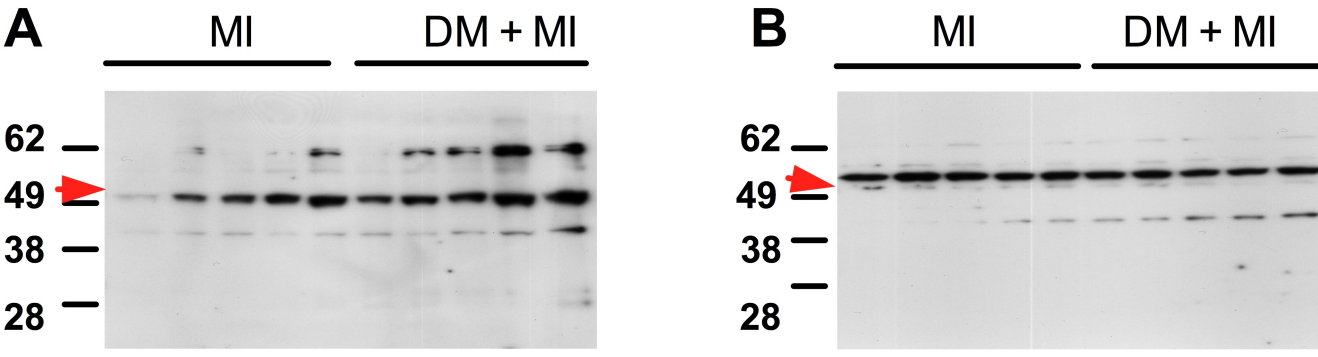

Full unedited gel for Figure 3B

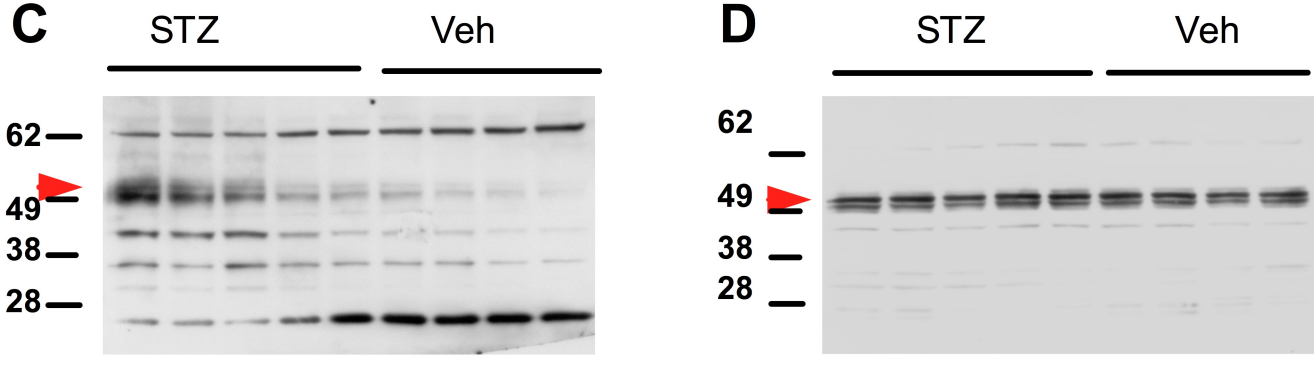

Western blot for Figure 3 A, B. ox-CaMKII (A, C) and CaMKII (B, D) staining of human and mice right atrial samples. Red arrow denotes ox-CaMKII or CaMKII.

Full unedited gel for Figure 4A

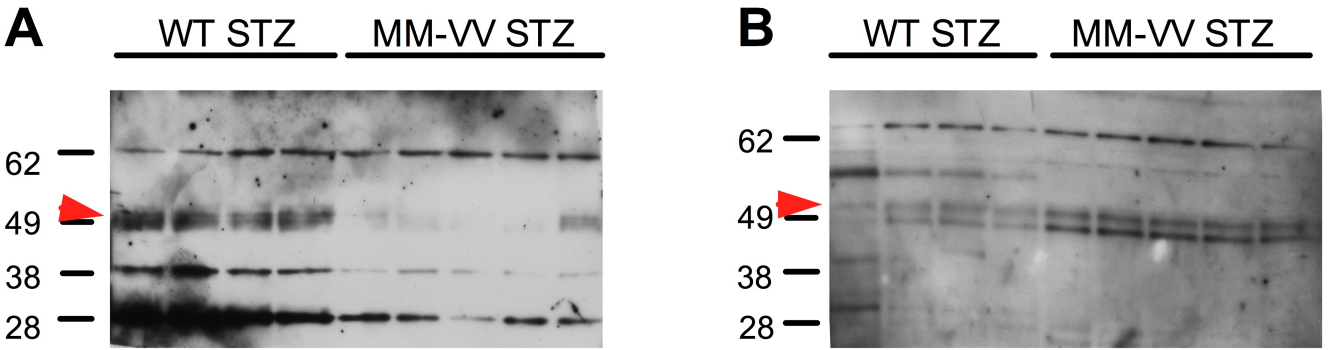

Western blot for Figure 4A. ox-CaMKII (A) and CaMKII (B) staining of right atrial samples from WT and MM-VV mice. Red arrow denotes ox-CaMKII or CaMKII.